Terahertz diffractive imaging with saturated data inpainting

Elizaveta G Tsiplakova, Jean-Baptiste Perraud, Adrien Chopard, Jean-Paul Guillet, Patrick Mounaix, Nikolay V Petrov

Terahertz Diffractive Imaging with Saturated Data Inpainting

ELIZAVETA G. TSIPLAKOVA[1] , JEAN-BAPTISTE PERRAUD[2] , ADRIEN CHOPARD[2,3] , JEAN-PAUL GUILLET[2] , PATRICK MOUNAIX[2] , AND NIKOLAY V. PETROV[1,4*]

[1]*Institute of Photonics and Optical Information Technologies, ITMO University, Kronverkskiy 49, 197101 Saint-Petersburg, Russia*
[2]*IMS Laboratory, University of Bordeaux, UMR CNRS 5218, 351 Cours de la Libération Bâtiment A31, 33405 Talence, France*
[3]*Lytid SAS, 8 rue la Fontaine, 92120 Montrouge, France*
[4]*Qingdao Innovation and Development Center, Harbin Engineering University, Qingdao, 266000 Shan-dong, China*
[*]*Corresponding author: n.petrov@niuitmo.ru*

Compiled November 20, 2023

Multiplane iterative phase retrieval is a promising approach to diffraction imaging, which accurately determines the topographic and internal characteristics of various objects. Nevertheless, the detection systems used often have a limited dynamic range, resulting in overexposure of recorded intensity distributions. In this Letter, we present a novel reconstruction algorithm that inpaints saturated areas on the measured intensity datasets and reliably retrieves wave complex amplitude. The proposed technique can be used in various spectral ranges, while we have tested it in the terahertz frequency range, where the problem of sources and detectors is the most acute. We show that retrieved amplitude and phase distributions have a quality comparable to that of the images reconstructed from the reference high dynamic range technique. Herewith, the proposed approach seriously simplifies process of data acquisition, what expands the possibilities in the design of measurement tools and studies of dynamic scenes.

http://dx.doi.org/10.1364/ao.XX.XXXXXX

Terahertz (THz) Phase imaging techniques with continuous wave (CW) sources are widely adopted in industrial applications due to the ease of experimental implementation and non-complex detection system in comparison with pulsed methods [1, 2]. Reconstructed information on phase delay provided by these techniques, is useful for determining topographic properties of samples [3], hidden structures of optically opaque dielectric objects [4, 5], and may serve as an input for tomographic reconstruction [6]. Many CW phase measurement techniques are applied with THz radiation: digital holography [7–11], interferometry [12, 13], transport of intensity equation (TIE) [14] and iterative phase retrieval (IPR) [15]. The last from the mentioned ones approaches include ptychography [16, 17] and multiple-plane algorithms such as the Single Beam Multiple Intensity Reconstruction (SBMIR) [4, 5, 18, 19] algorithm.

One of the problems which occurs in conducting measurements for phase retrieval and which especially manifests itself in THz range is associated with low dynamic range of detection systems. Using a detector with a dynamic range less than the intensity range of a signal results in overexposure. For instance, it was proposed to use CCD sensor to visualize THz radiation [20], however, due to its strong nonlinear response and low dynamic range the measured signal quickly go into saturation as the field amplitude increases. In addition, saturated regions occur when measuring the set of intensity distributions in reflective mode for wavefront retrieval of the object that contains both highly specular and diffuse regions. The first ones reflect parts of the incident beam with high intensity, while the latter scatter the radiation over a large solid angle, resulting in a significant reduction of the detected intensity in those regions. The conventional approach to address this problem is the high dynamic range (HDR) imaging. It relies on capturing multiple images of the same scene at different exposure levels, and then combining them into a single image with a greater dynamic range. HDR technique has already been successfully implemented in the visible range in off-axis [21] and phase-shifting digital holography [22], interferometric measurements [23] and shearography [24], while we adopted it for THz phase retrieval in reflection [18]. However, when using modern express data acquisition systems [19], HDR may not be practical for dynamic scenes. Therefore, in this work, we propose a new SBMIR-I iterative algorithm which inpaints saturated areas in the acquired data used for THz computational imaging and thus exactly retrieves the whole phase distribution of the object wave. (The letter 'I' in the algorithm title denotes 'Inpainting'. The underlying idea of this algorithm develops the concept of post-processing methods in coherent diffraction imaging [25], which have been implemented for the resolution enhancement [25–28] and signal-to-noise ratio improvement [29]. Herewith, according to our knowledge, this is the first work on algorithmic overexposure correction in THz diffractive imaging.

The flowchart of SBMIR-I algorithm is shown in Fig. 1. The algorithm requires input data in the form of two-dimensional

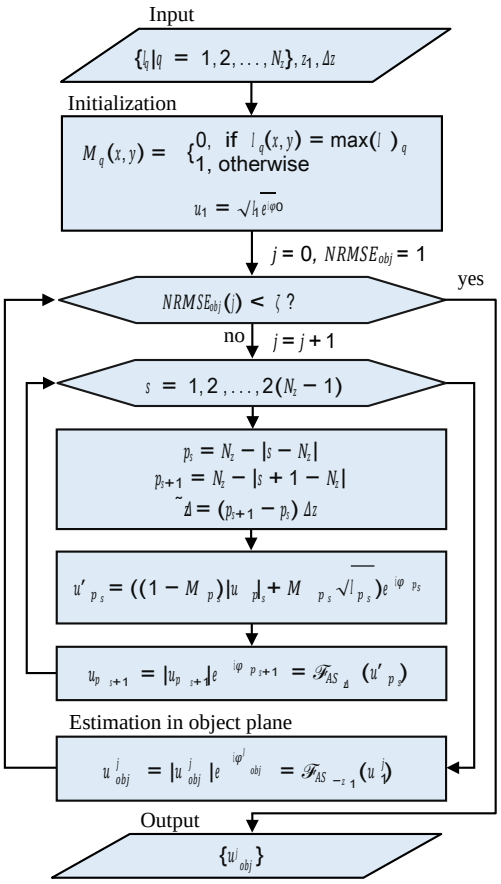

Fig. 1. Iterative procedure of SBMIR-I

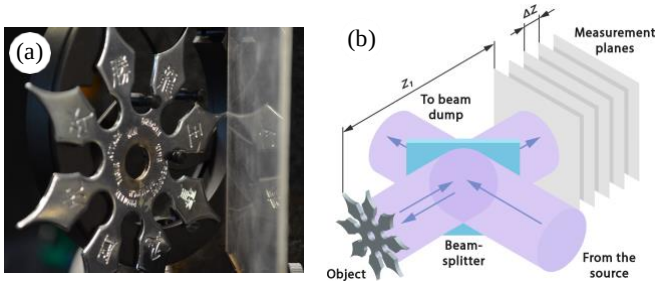

Fig. 2. (a) Photo of studied object (b) Scheme of a data acquisition setup

diffractive intensity distributions $\{I_q | q = 1, 2, ..., N_z\}$ with saturated areas. These diffraction patterns are spaced apart by Δz, with the first measurement plane positioned at a distance z_1 from the object. During initialization, the complex amplitude u_1 in the first measurement plane is estimated as the square root of recorded intensity I_1 and a constant phase φ_0. Binary masks $\{M_q | q = 1, 2, ..., N_z\}$ are then created to exclude saturated areas. The algorithm has two loops, one by the variable s for enumerating data registration planes forward and reverse, and another by the variable j for iteration number definition. The total number of transitions between each pair of neighbouring planes equals to $2(N_z-1)$. Variables p_s and p_{s+1} represent the current and subsequent planes, respectively and define the sign before the Δz (Δz). SBMIR-I, similar to the original SBMIR algorithm [18], keeps the phase estimates φ_{p_s}. It replaces amplitudes with the square root of measured intensities I_{p_s}, excluding saturated areas using the binary mask M_{p_s}. To describe propagation between two arbitrary planes separated by Δz, the angular spectrum operator $F_{AS_{\Delta z}}$ is introduced. Performing the internal loop results in an estimate of the complex amplitude in the first measurement plane. To calculate wavefield estimate in the object plane, u_1^j is propagated by a distance $(-z_1)$, resulting in the object field approximation u_{obj}^j at iteration j. The output of the algorithm is the array u_{obj}^j containing estimates in the object plane for each iteration.The minimum value ζ of the normalized root mean square error ($NRMSE$) serves as the stopping criteria for the iterative algorithm. Having at hand the amplitude distribution at the object plane obtained at the J^{th}-iteration with HDR technique as a reference function $|u_{obj_{HDR}}^J|$, we compared it with the reconstructed amplitude distribution at the specific iteration $|u_{obj}^j|$ to calculate $NRMSE_{obj}$. However, a more general practice in phase retrieval is to calculate the $NRMSE_{diffr}$ based on the unsaturated areas of the calculated diffraction patterns (see Section 1 of Supplement 1 for details). The value of ζ can vary depending on factors such as the object size and the extent of data saturation.

For experimental validation of proposed algorithm and its performance examination we used diffraction patterns recorded in the work [18], where several multi-distance datasets were obtained, including the dataset containing saturated areas and the HDR dataset, that we used as a reference. The measurement was performed in reflection mode with a beamsplitter and a shuriken employed as an object (Fig. 2 (a)). The scheme of intensity distributions recording for SBMIR-I is shown in Fig. 2 (b). A Gunn diode with frequency multiplication chain used as a source of THz radiation (0.287 THz, 14 mW power) and experimental data acquisition was carried out with a Schottky diode detector (SD) in a raster-scan mode, the signal from which was directed onto the LIA. Measurements were performed in $N_z = 27$ planes with the following acquisition parameters: the distance between the object plane and the first recording plane $z_1 = 83$ mm; longitudinal step $\Delta z = 5$ mm of the detector translation; the pixel pitch Δx, $\Delta y = 0.5$ mm; number of pixels in the spatial grid N_x, $N_y = 240$. For HDR dataset formation, two separate recordings of intensities were performed with two 30 dB LIAs of fixed voltages at 20 mV and 500 mV. Here, we use only one of these datasets, which contains images with saturated areas and was obtained with 20 mV fixed voltage LIA (Fig. 3 (a)). The set of binary masks, as well their inversions were designed for this dataset (Fig. 3 (b)). Then, the approximations of the missed central parts of diffracted wave field were retrieved by SBMIR-I algorithm, as shown in Fig. 3 (d). The amplitude values at this set are represented in the same range as in the reference HDR dataset, provided in Fig. 3 (e). The efficiency of inpainting in the central areas of the overexposed dataset is evidenced by the correspondence between the inpainted and the HDR cross-section graphs (Fig. 3 (c)), drawn through the center of amplitude distributions (Fig. 3 (a, d, e)).

To quantify the degree of saturation of a particular q diffraction pattern ($q = 1, 2, ..., N_z$), we introduced the parameter R_q. It represents the ratio of the integral intensity radiated into the saturation region $|u_q|(1 - M_q)^2$ to the total intensity $|u_q|^2$ reaching

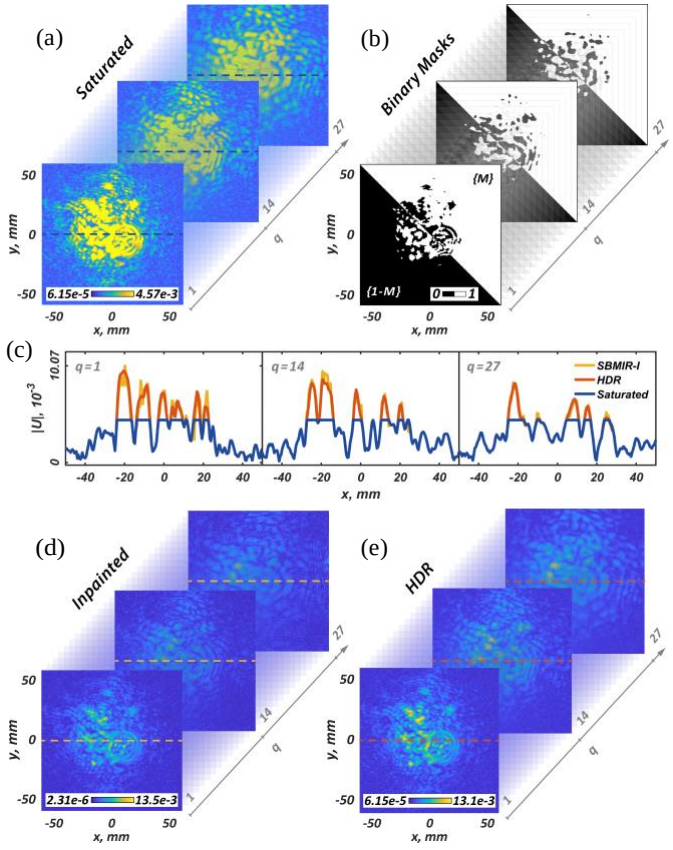

Fig. 3. The datasets of amplitude distributions extracted from the saturated intensities (a); the corresponding binary masks $\{M\}$ and $\{1-M\}$(b); inpainted in SBMIR-I procedure (d) and obtained with HDR technique (e) amplitudes. The cross-sections (c), drawn through the center of the amplitude distributions (a, d, e), are shown for the measurement planes with sequence numbers $q = 1, 14, 27$.

the sensor, including the saturation region:

$$R_q = \frac{\sum_{x,y=1}^{N_x,N_y} |u_q|(1-M_q)^2}{\sum_{x,y=1}^{N_x,N_y} |u_q|^2}. \quad (1)$$

This parameter quantifies the energy of the diffraction pattern that is lost due to saturation. In our experiment it was estimated from the HDR dataset, setting $u_q = u_{q_{HDR}}$. However, in real applications it can be approximately estimated after executing the SBMIR-I algorithm by calculating the intensities based on inpainted amplitude distributions. The results of R_q estimations range between 0.55 and 0.38 for the first and the last diffraction patterns in the dataset, respectively. In Section 2 of Supplement 1 we provide the numerical investigation of SBMIR-I convergence with an increase of intensity saturation in diffraction patterns. It was shown that even in case $R = 0.95$ the amplitude and phase in the object plane can be reconstructed, however it requires the increased number of iterations.

The reconstructed in the object plane phase φ_{obj} and amplitude $|u_{obj}|$ distributions are displayed in the top and in the middle rows of Fig. 4, respectively. The left and central columns display the reconstruction images using SBMIR and SBMIR-I from the saturated data, while the right column presents the wavefront distributions $u^J_{obj_{HDR}}$ reconstructed at $J = 9000$ iteration

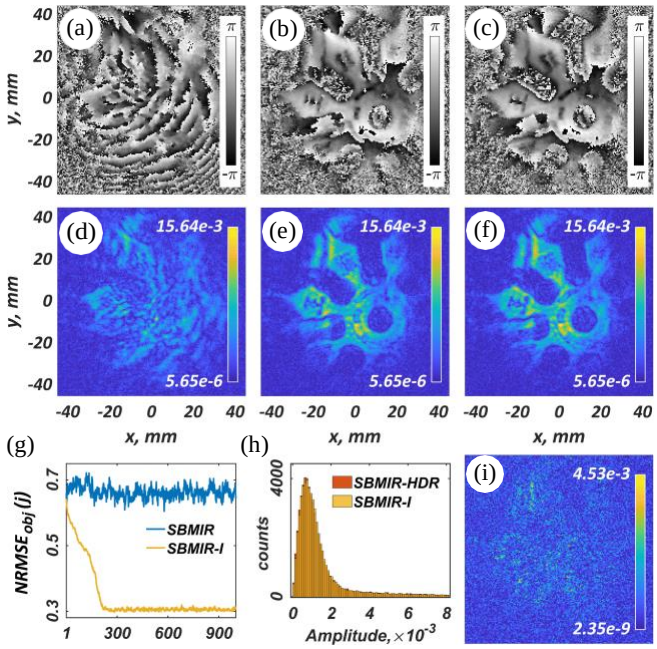

Fig. 4. Reconstructed phase (top row) and amplitude (middle row) distributions by SBMIR (a, d, c, f) and SBMIR-I (b, e) from saturated (a, b, d, e); and HDR (c, f) datasets. The bottom row displays $NRMSE_{obj}(j)$, showing the performance of SBMIR and SBMIR-I algorithms on the saturated dataset (g); histograms (h) of the amplitudes, displayed in (e) and (f), and their difference $|u_{obj} - u_{obj_{HDR}}|$(i).

from HDR dataset using SBMIR, which we used as a 'ground truth' approximations. The phases (a, b) and the corresponding amplitudes (d, e) were selected based on the minimum achieved error metric value for display in Fig. 4. Figure 4 (g) presents the $NRMSE_{obj}(j)$ graphs characterizing the performance of SBMIR and SBMIR-I on saturated data. The SBMIR algorithm failed to converge on the saturated dataset, whereas SBMIR-I achieved an infimum ζ value of 0.3 for the $NRMSE_{obj}$ after approximately 250 iterations, enabling field reconstruction of similar quality as the HDR technique. This is confirmed by the small spread of values in the amplitude difference $|u^J_{obj} - u^J_{obj_{HDR}}|$, as seen in Fig. 4 (i), and by the histograms shown in Fig. 4 (h), which are plotted based on the distributions (e) and (f). When constructing a histogram we limited the bin values by $8\ 10^3$, as the frequency of data points within the bins with higher values was small and did not exceed 50.

Discussing the practical relevance of the proposed algorithm, we would like to note that SBMIR-I has the ability to solve the problem of low dynamic range measurements without additional time or equipment required for conventional HDR imaging. This problem implies that the values of the scattered radiation intensities exceed the dynamic range of the detection system. One of the possible consequences of data acquisition in these conditions is the correct recording of strong central maximum at low sensitivity (short exposure) settings, which is accompanied by the fact that weak scattered radiation components become indistinguishable against the background of noise. Another possible outcome is the detection of the weak components at high sensitivity setting, which leads to the saturation of the high-intensity regions. The latter one is more expedient,

since high-intensity components of radiation are usually dispersed in a smaller solid angle and it is more problematic to reconstruct an image using them alone, while the application of the SBMIR-I algorithm provides reliable inpainting of the saturated areas in measured dataset and allows reconstructing the wavefront with a level of quality comparable to that of images recovered by the SBMIR algorithm from the HDR dataset [18]. Indeed, high spatial frequencies, which are generally involved in the high-quality wavefront reconstruction, has low intensity and deviate by a greater angle from the optical axis during wavefront propagation. Especially it applies to THz frequency range, because of the longer wavelength in comparison to optical range radiation. Therefore, it is more reliable to record the periphery of the wavefront (high spatial frequencies) and inpaint the lost central areas containing low spatial frequencies. In analyzing the distinctive features of SBMIR-I algorithm, it should be noted that the similar works [25–28] primarily focused on reconstructing high spatial frequency components to enhance resolution, while the object wavefield could be restored even without extrapolation procedure (albeit with a lower resolution). In present work, instead of the problem of low spatial resolution, the phase reconstruction problem is set, which solution is impossible with the use of saturated dataset and by means the algorithms proposed in works [25–28].

In the broad context of THz imaging, the proposed technique can be adapted to the other phase retrieval methods, which leverages multiple diffraction patterns, such as ptychography. In holography and single-plane IPR, the inpainting within a missing central part of the distribution is challenging [30]. Unlike these techniques, SBMIR-I offers a solution to the problem of missing center in saturated diffraction patterns and reconstructs the object phase distribution, using a multi-plane approach.

In conclusion, a multi-plane iterative phase retrieval algorithm was proposed that allows inpainting of the saturated areas on the intensity distributions and ensures reliable reconstruction of the object wavefront. Given algorithm was approved in THz frequency range on the experimental dataset which was acquired in the reflection mode and contained overexposured areas due to the hardware limitation of the dynamic range of the used detection system in 30 dB, while the whole signal range was around 45.6 dB. The performance of the proposed algorithm was compared with the performance of the conventional SBMIR algorithm in identical conditions in the processing of the saturated dataset. The amplitude image retrieved by SBMIR algorithms from the reference HDR dataset [18] is utilized for quantitative evaluation and *NRMSE* value was found for the amplitude reconstructed by SBMIR-I to be equal to 0.3. Herewith, the retrieved amplitude and phase distributions have the quality comparable with the reference HDR images. Thus, the simplification of data acquisition process in comparison to HDR technique is achieved, as SBMIR-I uses the single dataset, and the missed information in overexposed areas is inpainted, while HDR-merged dataset requires the conducting of at least two LIAs with complementary sensitivity setting. Thus, the developed algorithm allows overcoming the problem of limited dynamic range of detector more simply and reliable, since the use of HDR technologies is often impractical, especially in moving scenes.

The developed approach may be applied not only in THz region but in other spectral ranges, and allows to ease the examination of complex objects, including reflective ones, by means of phase retrieval. It is also worth mentioning that image inpainting has nowadays become a very vibrant research topic, driven by recent advancements in artificial intelligence (AI) and stable diffusion models. In this regard, the integration of AI in image inpainting could be considered as a very promising direction of further research.

Funding.

Disclosures. The authors declare no conflicts of interest.

REFERENCES

1. N. V. Petrov, M. S. Kulya, A. N. Tsypkin, V. G. Bespalov, and A. Gorodetsky, IEEE Transactions on Terahertz Sci. Technol. **6**, 464 (2016).
2. N. V. Petrov, B. Sokolenko, M. S. Kulya, A. Gorodetsky, and A. V. Chernykh, Light. Adv. Manuf. **3**, 1 (2022).
3. E. G. Tsiplakova, A. Chopard, N. S. Balbekin, O. A. Smolyanskaya, J. B. Perraud, J.-P. Guillet, P. Mounaix, and N. V. Petrov, Comput. Opt. (2023). (Submitted revision).
4. L. Valzania, P. Zolliker, and E. Hack, Optica. **6**, 518 (2019).
5. M. Agour, C. Falldorf, F. Taleb, M. Koch, R. B. Bergmann, and E. Castro-Camus, Opt. Lett. **47**, 3283 (2022).
6. D. Wang, X. Jin, J. Zhao, Y. Wang, L. Rong, and J. J. Healy, Chin. Opt. Lett. **19**, 123701 (2021).
7. R. J. Mahon, J. A. Murphy, and W. Lanigan, Opt. Commun. **260**, 469 (2006).
8. P. Zolliker and E. Hack, Opt. Express **23**, 10957 (2015).
9. M. Locatelli, M. Ravaro, S. Bartalini, L. Consolino, M. S. Vitiello, R. Cicchi, F. Pavone, and P. De Natale, Sci. Rep. **5**, 13566 (2015).
10. K. Xue, Q. Li, Y.-D. Li, and Q. Wang, Opt. Lett. **37**, 3228 (2012).
11. Y. Choporova, B. Knyazev, and V. Pavelyev, Light. Adv. Manuf. **3**, 525 (2022).
12. Y. Wang, Z. Zhao, Z. Chen, L. Zhang, K. Kang, and J. Deng, Appl. Opt. **50**, 6452 (2011).
13. J.-Y. Lu, C.-C. Kuo, C.-M. Chiu, H.-W. Chen, Y.-J. Hwang, C.-L. Pan, and C.-K. Sun, Opt. Express **16**, 2494 (2008).
14. L. Rong, S. Wang, D. Wang, F. Tan, Y. Zhang, J. Zhao, and Y. Wang, Opt. Lett. **46**, 5846 (2021).
15. N. V. Petrov, A. A. Gorodetsky, and V. G. Bespalov, Proc. SPIE **8846**, 88460S (2013).
16. L. Valzania, T. Feurer, P. Zolliker, and E. Hack, Opt. Lett. **43**, 543 (2018).
17. L. Rong, C. Tang, Y. Zhao, F. Tan, Y. Wang, J. Zhao, D. Wang, and M. Georges, Opt. Lett. **45**, 4412 (2020).
18. N. V. Petrov, J.-B. Perraud, A. Chopard, J.-P. Guillet, O. A. Smolyanskaya, and P. Mounaix, Opt. Lett. **45**, 4168 (2020).
19. A. Chopard, E. Tsiplakova, N. Balbekin, O. Smolyanskaya, J.-B. Perraud, J.-P. Guillet, N. V. Petrov, and P. Mounaix, Appl. Phys. B **128**, 63 (2022).
20. O. Chefonov, A. Ovchinnikov, M. Agranat, and A. Stepanov, Opt. Lett. **44**, 4099 (2019).
21. R. Yonesaka, Y. Lee, P. Xia, T. Tahara, Y. Awatsuji, K. Nishio, and O. Matoba, IEEE Transactions on Ind. Informatics **12**, 1658 (2016).
22. Y. Wu, J. P. Ryle, S. Liu, D. P. Kelly, and A. Stern, Appl. Opt. **54**, 3991 (2015).
23. J. Vargas, R. Restrepo, J. A. Quiroga, and T. Belenguer, Opt. Commun. **284**, 4141 (2011).
24. R. M. Groves, G. Pedrini, and W. Osten, Appl. Opt. **47**, 5550 (2008).
25. T. Latychevskaia and H.-W. Fink, Opt. Express **21**, 7726 (2013).
26. L. Rong, T. Latychevskaia, D. Wang, X. Zhou, H. Huang, Z. Li, and Y. Wang, Opt. Express **22**, 17236 (2014).
27. N. S. Balbekin, M. S. Kulya, A. V. Belashov, A. Gorodetsky, and N. V. Petrov, Sci. Rep. **9**, 1 (2019).
28. Z. Huang, C. Kuang, L. Xu, and L. Cao, Opt. Commun. **481**, 126526 (2021).
29. N. V. Petrov, N. S. Balbekin, M. S. Kulya, and A. A. Gorodetsky, Proc. SPIE **10677**, 1067721 (2018).
30. T. Latychevskaia, Opt. Commun. **452**, 56 (2019).

FULL REFERENCES

1. N. V. Petrov, M. S. Kulya, A. N. Tsypkin, V. G. Bespalov, and A. Gorodetsky, "Application of terahertz pulse time-domain holography for phase imaging," IEEE Transactions on Terahertz Sci. Technol. **6**, 464–472 (2016).
2. N. V. Petrov, B. Sokolenko, M. S. Kulya, A. Gorodetsky, and A. V. Chernykh, "Design of broadband terahertz vector and vortex beams: Ii. holographic assessment," Light. Adv. Manuf. **3**, 1–13 (2022).
3. E. G. Tsiplakova, A. Chopard, N. S. Balbekin, O. A. Smolyanskaya, J. B. Perraud, J.-P. Guillet, P. Mounaix, and N. V. Petrov, "The algorithm of unordered wavefront propagation in terahertz phase retrieval with dense multiplane data acquisition," Comput. Opt. (2023). (Submitted revision).
4. L. Valzania, P. Zolliker, and E. Hack, "Coherent reconstruction of a textile and a hidden object with terahertz radiation," Optica. **6**, 518–523 (2019).
5. M. Agour, C. Falldorf, F. Taleb, M. Koch, R. B. Bergmann, and E. Castro-Camus, "Chocolate inspection by means of phase-contrast imaging using multiple-plane terahertz phase retrieval," Opt. Lett. **47**, 3283–3286 (2022).
6. D. Wang, X. Jin, J. Zhao, Y. Wang, L. Rong, and J. J. Healy, "Continuous-wave terahertz diffraction tomography for measuring three-dimensional refractive index maps," Chin. Opt. Lett. **19**, 123701 (2021).
7. R. J. Mahon, J. A. Murphy, and W. Lanigan, "Digital holography at millimetre wavelengths," Opt. Commun. **260**, 469–473 (2006).
8. P. Zolliker and E. Hack, "Thz holography in reflection using a high resolution microbolometer array," Opt. Express **23**, 10957–10967 (2015).
9. M. Locatelli, M. Ravaro, S. Bartalini, L. Consolino, M. S. Vitiello, R. Cicchi, F. Pavone, and P. De Natale, "Real-time terahertz digital holography with a quantum cascade laser," Sci. Rep. **5**, 13566 (2015).
10. K. Xue, Q. Li, Y.-D. Li, and Q. Wang, "Continuous-wave terahertz in-line digital holography," Opt. Lett. **37**, 3228–3230 (2012).
11. Y. Choporova, B. Knyazev, and V. Pavelyev, "Holography with high-power cw coherent terahertz source: optical components, imaging, and applications," Light. Adv. Manuf. **3**, 525 (2022).
12. Y. Wang, Z. Zhao, Z. Chen, L. Zhang, K. Kang, and J. Deng, "Continuous-wave terahertz phase imaging using a far-infrared laser interferometer," Appl. Opt. **50**, 6452–6460 (2011).
13. J.-Y. Lu, C.-C. Kuo, C.-M. Chiu, H.-W. Chen, Y.-J. Hwang, C.-L. Pan, and C.-K. Sun, "Thz interferometric imaging using subwavelength plastic fiber based thz endoscopes," Opt. Express **16**, 2494–2501 (2008).
14. L. Rong, S. Wang, D. Wang, F. Tan, Y. Zhang, J. Zhao, and Y. Wang, "Transport of intensity equation-based terahertz lensless full-field phase imaging," Opt. Lett. **46**, 5846–5849 (2021).
15. N. V. Petrov, A. A. Gorodetsky, and V. G. Bespalov, "Holography and phase retrieval in terahertz imaging," Proc. SPIE **8846**, 88460S (2013).
16. L. Valzania, T. Feurer, P. Zolliker, and E. Hack, "Terahertz ptychography," Opt. Lett. **43**, 543–546 (2018).
17. L. Rong, C. Tang, Y. Zhao, F. Tan, Y. Wang, J. Zhao, D. Wang, and M. Georges, "Continuous-wave terahertz reflective ptychography by oblique illumination," Opt. Lett. **45**, 4412–4415 (2020).
18. N. V. Petrov, J.-B. Perraud, A. Chopard, J.-P. Guillet, O. A. Smolyanskaya, and P. Mounaix, "Terahertz phase retrieval imaging in reflection," Opt. Lett. **45**, 4168–4171 (2020).
19. A. Chopard, E. Tsiplakova, N. Balbekin, O. Smolyanskaya, J.-B. Perraud, J.-P. Guillet, N. V. Petrov, and P. Mounaix, "Single-scan multiplane phase retrieval with a radiation of terahertz quantum cascade laser," Appl. Phys. B **128**, 63 (2022).
20. O. Chefonov, A. Ovchinnikov, M. Agranat, and A. Stepanov, "Terahertz beam spot size measurements by a ccd camera," Opt. Lett. **44**, 4099–4102 (2019).
21. R. Yonesaka, Y. Lee, P. Xia, T. Tahara, Y. Awatsuji, K. Nishio, and O. Matoba, "High dynamic range digital holography and its demonstration by off-axis configuration," IEEE Transactions on Ind. Informatics **12**, 1658–1663 (2016).
22. Y. Wu, J. P. Ryle, S. Liu, D. P. Kelly, and A. Stern, "Experimental evaluation of inline free-space holography systems," Appl. Opt. **54**, 3991–4000 (2015).
23. J. Vargas, R. Restrepo, J. A. Quiroga, and T. Belenguer, "High dynamic range imaging method for interferometry," Opt. Commun. **284**, 4141–4145 (2011).
24. R. M. Groves, G. Pedrini, and W. Osten, "Real-time extended dynamic range imaging in shearography," Appl. Opt. **47**, 5550–5556 (2008).
25. T. Latychevskaia and H.-W. Fink, "Resolution enhancement in digital holography by self-extrapolation of holograms," Opt. Express **21**, 7726–7733 (2013).
26. L. Rong, T. Latychevskaia, D. Wang, X. Zhou, H. Huang, Z. Li, and Y. Wang, "Terahertz in-line digital holography of dragonfly hindwing: amplitude and phase reconstruction at enhanced resolution by extrapolation," Opt. Express **22**, 17236–17245 (2014).
27. N. S. Balbekin, M. S. Kulya, A. V. Belashov, A. Gorodetsky, and N. V. Petrov, "Increasing the resolution of the reconstructed image in terahertz pulse time-domain holography," Sci. Rep. **9**, 1–9 (2019).
28. Z. Huang, C. Kuang, L. Xu, and L. Cao, "Multiplane digital holography based on extrapolation iterations," Opt. Commun. **481**, 126526 (2021).
29. N. V. Petrov, N. S. Balbekin, M. S. Kulya, and A. A. Gorodetsky, "Reconstruction enhancement of noisy data in terahertz pulse time-domain holography by iterative procedure," Proc. SPIE **10677**, 1067721 (2018).
30. T. Latychevskaia, "Reconstruction of missing information in diffraction patterns and holograms by iterative phase retrieval," Opt. Commun. **452**, 56–67 (2019).